Planning and Controlling Cooperating Robots through Distributed Impedance

Jérôme Szewczyk,* Frédéric Plumet, and Philippe Bidaud
Laboratoire de Robotique de Paris 6
10/12, av. de l'Europe, 78140 Vélizy, France
e-mail: sz@robot.uvsq.fr

Received 10 June 2001; accepted 3 January 2002

This article presents distributed impedance as a new approach for multiple robot system control. In this approach, each cooperating manipulator is controlled by an independent impedance controller. In addition, along selected degrees of freedom, force control is achieved through an external loop, to improve control of the object's internal loading. Extensive stability analysis is performed, based on a realistic model that includes robot impedance and object dynamics. Experiments are performed using two cooperating industrial robots holding an object through point contacts. Force and position control actions are suitably dispatched to achieve both internal loading control and object position control. Individual impedance parameters are specified according to the theoritical stability criterion. The performance of the system is demonstrated for transportation and contact tasks.

1. INTRODUCTION

The coordination of several manipulators is frequently considered in the manipulation of heavy or large objects. It may also be required for the manipulation of nonrigid bodies or to perform complex assembly tasks. In such cases, the system performance depends on each individual subsystem performance.

Dexterous articulated hands also belong to the coordinated system family. They offer a high degree of flexibility in grasp configuration, and can be used to impart fine motions to the grasped object. In such systems the fingers can be viewed as small manipulators and the contacts as the effectors.

The coordination problem of manipulators can be split in two subproblems :

1. trajectory tracking for free or constrained motions of the object,
2. internal forces control under contact stability constraints.

*To whom all correspondence should be addressed.

1.1. Previous Works

Most approaches previously proposed for coordinated manipulation control can be divided into three categories:

1. object level control,
2. effector level control, and
3. joint level control.

The first considers the manipulators and the grasped object as a whole (Figure 1(a)). They can be viewed as extensions of operational space control to multi-manipulator systems.[1] Different control schemes have been adapted to this context, for example: hybrid force-position control,[2–5] computed torque control[6,7] and impedance control.[8–11]

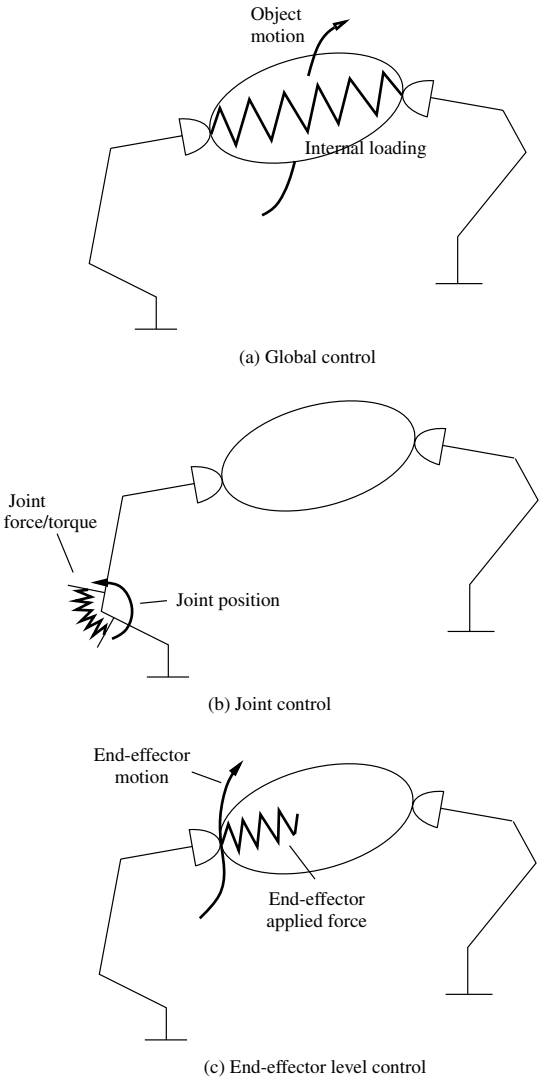

Figure 1. Control variables in different approaches to coordinated manipulation.

Such a centralized approach implies that specific pieces of hardware share data in real time from each manipulator force and position sensor. Notice that the structure of the controller depends on the system. This almost prohibits the implementation of regrasping procedures or, more generally, any change in the system topology.

Furthermore, when the system is built-up by manipulators with heterogeneous performance, the whole system performance reflects that of the worst one, especially for precision and stability.

An alternative to global control consists in considering each manipulator as autonomous and independently controlled. This greatly simplifies the implementation of the coordinated control. From the hardware point of view, each manipulator controller keeps its original individual structure. Changes in system topology are easier and do not lead to significant modifications in control structure. Obviously, this modularity gives more flexibility in the use of the coordinated manipulation system. Furthermore, system performance optimization can be addressed through performance optimization of each individual manipulator. Phenomena (actuators dynamics, noncolocated modes, etc.) limiting the performance of a given manipulator can be dealt with locally, without major influence on the rest of the cooperative system.

A first possible approach (Figure 1(b)) for local control of multirobot systems is to use pure joint control.[12,13] In that case, hardware and software implementation are greatly simplified. However, since the task is controlled at the object level, it is necessary to invert the grasp models and manipulator kinematics.[14] This is why joint-level approaches are very sensitive to uncertainties in manipulators and grasp geometries.

An alternative is effector-level control (Figure 1(c)). Here we must deal with position and force control at the contact between the end-effectors and the manipulated object. Such an approach offers an interesting trade-off between the simplicity of joint-level solutions and the efficiency of centralized solutions. Moreover, important problems linked to point-contact manipulation (i.e., control of impact, sliding on object surface, etc.) can be addressed in a more direct and suitable manner.

Coordinated manipulation control at the end-effector level has been investigated for many years.

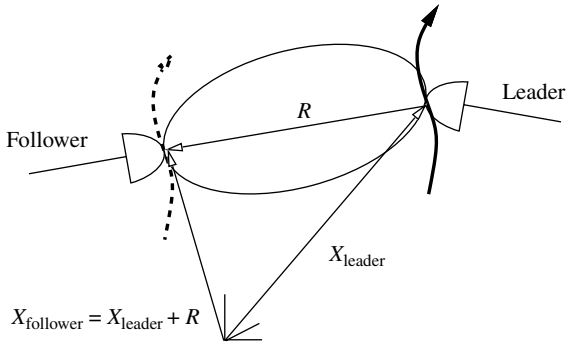

(a) Leader-follower solution

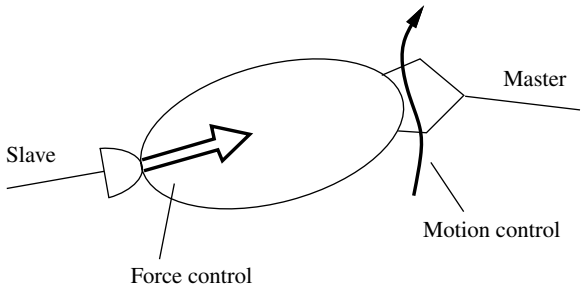

(b) Master-slave solution

Figure 2. Two solutions for effector-level control of coordinated manipulation.

In the leader-follower approach, for example,[13,15,16] one in two cooperating manipulators has its end-effector trajectory in-line adjusted with respect to the actual trajectory of the other (Figure 2(a)). For this, closed-chain kinematic constraints are explicitly taken into account. Internal forces that are not directly controlled entirely rely on exact knowledge of manipulated object compliance and geometry.

In the master-slave approach,[2,16] the master (which is position controlled) induces object motions, whereas the slave, (which is purely force controlled) must regulate internal forces while the object is in motion (Figure 2(b)). In that case, internal force regulation entirely relies on the loop rapidity of the slave force control.

More recently, the hybrid external solution has been proposed[17] to simultaneously control both force and position at each end-effector.[18] This symmetric solution provides flexibility and simplifies object internal and external applied force regulation. However, the force control action remains predominant (integral action) over the position control action. This makes the system unable to reject disturbances applied to the manipulated object.

1.2. The Distributed Impedance Approach

Effector-level control of coordinated manipulation must face two major difficulties simultaneously:

1. From each coordinated manipulator's point of view, the environment (the manipulated object and the other manipulators) reflects a complex dynamic behavior. Thus, from stability considerations, a local force controller cannot be implemented with an arbitrarily high gain. For that reason, master-slave solutions are not suitable for coordinated manipulation.
2. Because internal load regulation and trajectory control are fundamental components of coordinated manipulation, both forces and motion must be simultaneously and precisely controlled. As a consequence, it is not realistic to simply implement pure position control symmetrically on each manipulator (as in the leader-follower approach), nor to generalize closed-loop force control (as in the hybrid external approach[17]).

To overcome these difficulties, we propose the distributed impedance control approach. This approach is based on an individual impedance control of each manipulator.

Basically, impedance control establishes a linear relationship between the wrench applied to the end-effector $\mathbf{F}$ and the error between desired and actual end-effector configuration $\tilde{\mathbf{X}} - \mathbf{X}$. Thus, the manipulator will react in a limited and predictable way to any external disturbance. Robustness in impedance control has been slightly demonstrated (for instance in refs. 19 and 20). More generally, impedance control is well suited to the control of contact tasks involving a complex and dynamically variable environment.

Moreover, explicit force control can be locally added simply by activating an external force loop over the existing impedance scheme.[20,21] In the coordinated manipulation context, this can be particularly useful, because it is necessary to control both force and motion at the end-effector level accurately.

Impedance control has been proposed to control multiarm systems, but only in a semi-distributed way.[22,23] In both cases, information about robot positions and forces still needs to be centralized. In Bonitz and Hsia,[22] individual impedance control schemes take into account only the part of applied efforts producing internal load, and then introduce coupling effects between object motion and internal load regulation. In Kosuge et al.,[24] impedance distribution was

implemented using virtual internal model of the manipulator end-effectors. But there is no consideration of how impedances are distributed, nor how to introduce explicit force control in the object–end-effector interactions.

In the next section, a new distributed impedance control structure is proposed and developed for a set of manipulators grasping an object through simple point contacts. Object motion, internal force realization, and control are addressed, and a complete algorithm for computation of the corresponding individual reference trajectories and forces is proposed.

A stability analysis based on the hyperstability principle is developed in Section 3, giving sufficient conditions for the stability of the distributed impedance controller.

Section 4 provides experimental results to verify the ability of the distributed impedance approach to realize point-contact grasping tasks. A dynamic transporting task is first performed, then the object comes into contact with a stiff, planar environment with a desired applied effort. Both tasks illustrate the ability of impedance distribution to accurately control object trajectory and internal forces.

2. SYSTEM DESCRIPTION

Let us consider an object S_p grasped by n manipulators through frictional point contacts (Figure 3). $\mathcal{R}_o$ is a frame fixed to the object. For simplicity, its origin $\mathbf{O}^\circ$ is chosen to be the mass center of S_p. $\mathcal{R}_b$ is a base frame fixed to the environment. In the following, all vectors and matrices are expressed with respect to the vectors of $\mathcal{R}_b$.

The absolute configuration of $\mathcal{R}_o$ with respect to a base frame $\mathcal{R}_b$ is given by the 3×1 position vector $\mathbf{X}^\circ$ and the 3×3 rotation matrix ${}^\circ\mathbf{R}_b$. The generalized

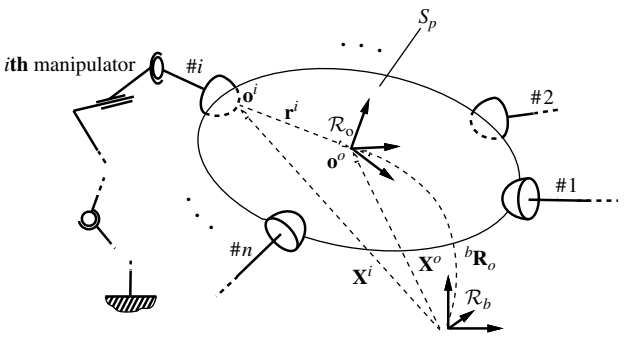

Figure 3. Grasp geometry.

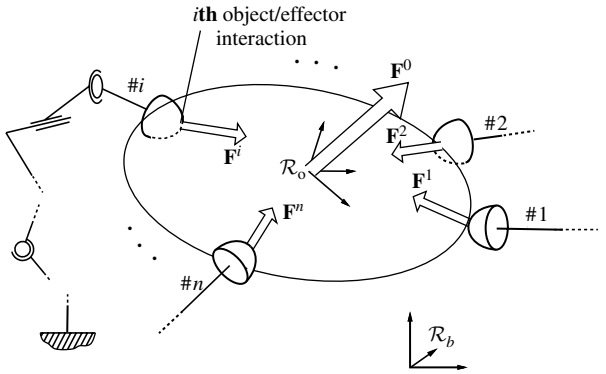

Figure 4. Object/effector interaction.

velocity of $\mathcal{R}_o$ is represented by the 6×1 vector $\mathbf{V}^\circ$:

$$\mathbf{V}^\circ = (\dot{\mathbf{X}}^{\circ\mathrm{T}}, \boldsymbol{\Omega}^{\circ\mathrm{T}})^{\mathrm{T}} \tag{1}$$

where $\dot{\mathbf{X}}^\circ = \frac{d\mathbf{X}^\circ}{dt}$ and $\boldsymbol{\Omega}^\circ$ is a 3×1 rotational velocity vector.

The ith effector contact point on the object is $\mathbf{O}^i$. Its location with respect to $\mathcal{R}_o$ is given by the constant 3×1 position vector $\mathbf{r}^i$. The position of $\mathbf{O}^i$ in $\mathcal{R}_b$ is represented by $\mathbf{X}^i$.

The object motion equation is

$$\mathbf{F}^{\mathrm{ext}} + \mathbf{F}^\circ = \boldsymbol{\Lambda}^\circ \dot{\mathbf{V}}^\circ + \mathbf{C}^\circ \tag{2}$$

$$\boldsymbol{\Lambda}^\circ = \begin{pmatrix} \mathrm{m}^\circ \mathbb{I}_3 & \mathbf{0}_3 \\ \mathbf{0}_3 & \mathrm{I}^\circ \end{pmatrix}$$

$$\mathbf{C}^\circ = \begin{pmatrix} -\mathrm{m}^\circ \mathbf{g} \\ \boldsymbol{\Omega}^\circ \times \mathrm{I}^\circ \boldsymbol{\Omega}^\circ \end{pmatrix}$$

where $\mathbb{I}_3$ is the 3×3 identity matrix and $\mathbf{0}_3$ is the 3×3 null matrix. $\mathbf{F}^\circ$ is the resultant force/moment vector applied to S_p at point $\mathbf{O}^\circ$ by the set of commanded end-effectors (Figure 4). $\mathbf{F}^{\mathrm{ext}}$ is the external force/moment vector at $\mathbf{O}^\circ$. $\mathbf{F}^{\mathrm{ext}} = \mathbf{0}$ when S_p has no contact with its environment. $\boldsymbol{\Lambda}^\circ$ is the object's generalized inertia matrix, built from its mass m° and inertia tensor I° expressed with respect to point $\mathbf{O}^\circ$ and the vectors of $\mathcal{R}_b$. $\mathbf{C}^\circ$ represents Coriolis and gravitational effects, constructed with the gravitational acceleration vector $\mathbf{g}$.

A pure force $\mathbf{F}^i$ is applied to the object through the ith contact point. The $\mathbf{F}^i$ are grouped into a $3n \times 1$ vector $\mathbf{F} = (\mathbf{F}^{1\mathrm{T}}, \ldots, \mathbf{F}^{n\mathrm{T}})^{\mathrm{T}}$. $\mathbf{F}$ is related to $\mathbf{F}^\circ$ through the $6 \times 3n$ grasp matrix $\mathbf{W}$:

$$\mathbf{F}^\circ = \mathbf{W}\,\mathbf{F} \tag{3}$$

For the vectors $\mathbf{F}$, $\mathbf{F}^\circ$, and $\mathbf{r}^i$, $(i = 1, \ldots, n)$ expressed

in the base frame $\mathcal{R}_b$ and with $\mathbf{O}^\circ$ as reduction point, we have

$$\mathbf{W} = \begin{pmatrix} \mathbb{I}_3 & \dots & \mathbb{I}_3 \\ -S(\mathbf{r}^1) & \dots & -S(\mathbf{r}^n) \end{pmatrix} \tag{4}$$

Where $S(\cdot)$ represents the cross-product operator.

The application of the principle of virtual work to Eq. (3) gives the vector of the individual end-effector velocities $\dot{\mathbf{X}} = (\dot{\mathbf{X}}^{1\mathrm{T}}, \dots, \dot{\mathbf{X}}^{n\mathrm{T}})^\mathrm{T}$:

$$\dot{\mathbf{X}} = \mathbf{W}^\mathrm{T} \left(\dot{\mathbf{X}}^{\circ\mathrm{T}},\ \boldsymbol{\Omega}^{\circ\mathrm{T}}\right)^\mathrm{T} = \mathbf{W}^\mathrm{T}\, \mathbf{V}^\circ \tag{5}$$

And for infinitesimal displacements $\boldsymbol{\delta}\mathbf{X}^\circ$ and $\boldsymbol{\delta}\mathbf{X} = (\boldsymbol{\delta}\mathbf{X}^{1\mathrm{T}}, \dots, \boldsymbol{\delta}\mathbf{X}^{n\mathrm{T}})^\mathrm{T}$, we have

$$\boldsymbol{\delta}\mathbf{X} = \mathbf{W}^\mathrm{T}\, \boldsymbol{\delta}\mathbf{X}^\circ \tag{6}$$

The object internal forces belong to the null space of $\mathbf{W}$. Assuming that $\mathbf{W}$ is a full-rank matrix, and that $\mathbf{N}$ is a $(3n) \times (3n-6)$ matrix whose columns form a base of the null space of $\mathbf{W}$, we have

$$\mathbf{F} = \mathbf{W}^\sharp\, \mathbf{F}^\circ + \mathbf{N}\, \boldsymbol{\eta}^\circ \tag{7}$$

where $\mathbf{W}^\sharp = \mathbf{W}^\mathrm{T} (\mathbf{W}\, \mathbf{W}^\mathrm{T})^{-1}$ is the right generalized inverse of $\mathbf{W}$. The first term in Eq. (7) represents the contribution of the contact forces to object manipulation; and $\boldsymbol{\eta}^\circ$ represents the $3n-6$ vector of the internal force magnitudes.

The selection of $\mathbf{N}$ and $\boldsymbol{\eta}^\circ$ significantly influences grasp stability. Possible choices of $\mathbf{N}$ and $\boldsymbol{\eta}^\circ$ are given in Section 5 for some simple grasp configurations. For more details the reader should refer to Nakamura et al.[25] and to Szewczyk and Bidaud.[26]

2.1. End-effector Control

In the distributed impedance control approach, each manipulator is driven by its own independent impedance controller. An impedance is specified for each end-effector participating in the task. This impedance links the ith component $\mathbf{F}^i$ of $\mathbf{F}$ to $\tilde{\mathbf{X}}^i$ and $\mathbf{X}^i$ (i.e., corresponding to reference and actual end-effector position vectors):

$$-\mathbf{F}^i = \mathbf{M}^i \ddot{\mathbf{X}}^i + \mathbf{B}^i (\dot{\mathbf{X}}^i - \dot{\tilde{\mathbf{X}}}^i) + \mathbf{K}^i (\mathbf{X}^i - \tilde{\mathbf{X}}^i) \tag{8}$$

Here $\mathbf{K}^i$, $\mathbf{B}^i$, and $\mathbf{M}^i$ are 3×3 diagonal matrices that define the ith individual target impedance. When controlling a single manipulator, they are specified according to local constraints, such as free or constrained directions, apparent end-effector inertia matrix, and so on.[21] When several manipulators are controlled, the $\mathbf{K}^i$, $\mathbf{B}^i$, and $\mathbf{M}^i$ matrices are also determined by the global impedance desired to reflect on the manipulated object.

The impedance behavior described by Eq. (8) can be obtained in different ways. Some solutions (such as position based impedance control[27]) rely on position control at the joint level. They do not allow an arbitrary choice of the target impedance parameters.[28] Other solutions (such as force based impedance control[29]), rely on control of the manipulator dynamics in its operational space. Actuator commanded forces f_{com} are computed, such as

$$\mathbf{J}^{i\,-\mathrm{T}}\, f^i_{\mathrm{com}} - \mathbf{F}^i = \boldsymbol{\Lambda}^i \ddot{\mathbf{X}}^i + \mathbf{C}^i \tag{9}$$

Here, $\mathbf{J}^i$ is the Jacobian matrix of the ith manipulator, which is assumed to be nonredundant and nonsingular. $\boldsymbol{\Lambda}^i$ and $\mathbf{C}^i$ are respectively the operational apparent inertia matrix, and the Coriolis, centrifugal, and gravitational forces.

According to Eqs. (8) and (9), we have

$$\begin{aligned} f^i_{\mathrm{com}} = \ & \mathbf{J}^{i\mathrm{T}} [\boldsymbol{\Lambda}^i\, \mathbf{M}^{i-1} (\mathbf{B}^i (\dot{\mathbf{X}}^i - \dot{\tilde{\mathbf{X}}}^i) + \mathbf{K}^i (\mathbf{X}^i - \tilde{\mathbf{X}}^i) \\ & + \mathbf{C}^i + (\mathbb{I}_3 - \boldsymbol{\Lambda}^i \mathbf{M}^{i-1})\, \mathbf{F}^i] \end{aligned} \tag{10}$$

which requires an on-line estimation of the applied effort $\mathbf{F}^i$. This solution has been chosen in this work. It has been implemented following the control scheme presented in Figure 5.

2.2. Reference Trajectories

Each individual impedance controller defined by Eq. (8) is featured with a unique input variable, which is the reference trajectory $\tilde{\mathbf{X}}^i$ computed according to task specification (i.e., desired object trajectory $\tilde{\mathbf{X}}^\circ$, ${}^\circ\tilde{\mathbf{R}}_\mathrm{b}$, $\tilde{\mathbf{V}}^\circ$, $\dot{\tilde{\mathbf{V}}}^\circ$, and internal load $\tilde{\boldsymbol{\eta}}^\circ$). Each individual reference trajectory can be viewed as the sum of an *accompanying* trajectory $\tilde{\mathbf{X}}^i_a$ and an *additional* trajectory $\tilde{\mathbf{X}}^i_+$ (Figure 6).

$\tilde{\mathbf{X}}^i_a$ is the ith contact-point trajectory required by the object desired motion, considering a given grasp geometry:

$$\tilde{\mathbf{X}}^i_a = \tilde{\mathbf{X}}^\circ - {}^\circ\tilde{\mathbf{R}}^\mathrm{T}_b\, \mathbf{r}^i \tag{11}$$

The additional trajectory $\tilde{\mathbf{X}}^i_+$ is aimed to generate the ith desired end-effector/object interaction force $\tilde{\mathbf{F}}^i$ (i.e., the contribution of the ith manipulator to the object internal forces, object dynamics compensation,

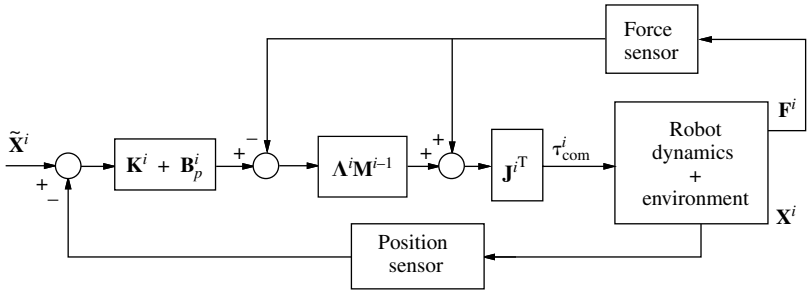

Figure 5. Force-based impedance control.

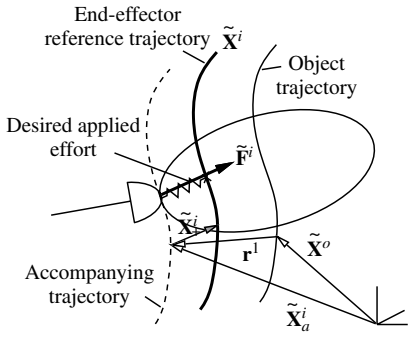

Figure 6. Composition of local reference trajectories.

and application of an external force $\mathbf{F}^{\mathrm{ext}}$). Namely, according to Eqs. (3) and (7), its value is

$$\tilde{\mathbf{F}}^i = \mathbf{u}^{i\mathrm{T}}\,\tilde{\mathbf{F}} \tag{12}$$

$$\tilde{\mathbf{F}} = (\tilde{\mathbf{W}}^{\sharp}\,(\tilde{\mathbf{\Lambda}}^{\circ}\,\dot{\tilde{\mathbf{V}}}^{\circ} + \tilde{\mathbf{C}}^{\circ}) + \tilde{\mathbf{N}}\,\tilde{\boldsymbol{\eta}}^{\circ}) \tag{13}$$

where $\mathbf{u}^{i\mathrm{T}} = (\mathbf{0}_{3\times 3(i-1)}, \mathbf{I\!I}_3, \mathbf{0}_{3\times 3(n-i+1)})$ is a suitable projection operator to extract $\tilde{\mathbf{F}}^i$ from $\tilde{\mathbf{F}}$. According to Eq. (8), $\tilde{\mathbf{X}}^i_+$ is finally deduced from $\tilde{\mathbf{F}}^i$ by the following low-pass filter application:

$$\tilde{\mathbf{X}}^i_+ = \mathcal{L}^{-1}\left(\frac{\mathcal{L}(\tilde{\mathbf{F}}^i)}{\mathbf{B}^i\,p + \mathbf{K}^i}\right) \tag{14}$$

where $\mathcal{L}(\cdot)$ represents the Laplace transformation and p represents the derivative operator.

2.3. Active Force Control

In distributed impedance control, the contact forces $\mathbf{F}^i$ are not explicitly controlled with a feedback loop. Instead, they are specified off-line through desired position terms $\tilde{\mathbf{X}}^i_+$ (see Eq. (14)) and applied in a feedforward manner. Thus, the system is unable to reject disturbances that make $\mathbf{F}^i$ deviate from its desired value $\tilde{\mathbf{F}}^i$. This is the case when the real end-effector stiffness $\mathbf{K}^i$ differs from its predicted value, used in Eq. (14) to derive $\tilde{\mathbf{X}}^i_+$. A mechanism that can control the end-effector contact forces and reject such disturbances is then much needed.

However, introducing complete active force control for all the $\mathbf{F}^i$ components would lead to a loss of control of object position. In this case, the system would be completely unable to reject any external force applied to the object (as explained in Section 1).

To solve this problem, we select only a subset of the $\mathbf{F}$ components that will be actively force controlled, while pure impedance control is maintained on the other components. The two different subsets include respectively n_φ and n_π end-effector/object interaction components, and $n_\pi + n_\varphi = 3n$. The $6 \times n_\pi$ grasp matrix ${}_\pi\mathbf{W}$ extracted from $\mathbf{W}$ is associated with the purely impedance controlled interaction components. ${}_\pi\mathbf{W}$ must be full rank to guarantee complete position control of the object. In the case of free spatial manipulations, $n_\pi \geq 6$ is implied; that necessary condition is the same as the force-closure condition derived by Nguyen.[30]

Theoretically, it is sufficient to choose six independent components to be position controlled ($n_\pi = 6$). Practically, $n_\pi > 6$ can be useful for preserving the rank of ${}_\pi\mathbf{W}$ from discrepancy and to facilitate apparent impedance conditioning of the object. However, in the following, we have chosen to restrict the number of purely impedance controlled interactions to the minimum ($n_\pi = 6$) to maximize the number of interaction components under force control.

The choice of n_φ and n_π, however, does not say *which* components of $\mathbf{F}$ should be force or purely impedance controlled. Note that it is more straightforward to select the n_φ force controlled components. The force controlled components are selected from the internal forces when the object is in free motion. For constrained motions of the object, these components

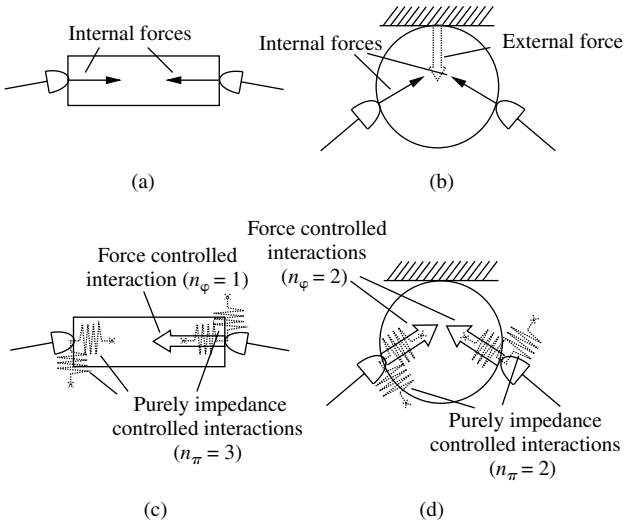

Figure 7. Example of force and pure impedance controller repartition.

are among those which also compensate the object interaction with the environment $\mathbf{F}^{\text{ext}}$. This is illustrated in Figure 7 for simple two-finger grasps.

The resulting distributed impedance control scheme, including active force control, is represented in Figure 8. Along the n_φ selected directions, force control is achieved using an external force loop,[20,21] which modifies the corresponding reference velocity proportionally to the measured force error.

Note that along each end-effector/object interaction component, selected to be either purely impedance controlled or force controlled, the original impedance controller (8) is still implemented. That clearly distinguishes between the distributed impedance control approach and the master/slave methods. In distributed impedance, the manipulator motion is always anticipated through the programmed trajectory $\mathbf{X}_a^i$ (Eq. (11)), even if a local force controller is implemented.

3. STABILITY STUDY

We consider that position and force control actions are distributed according to the considerations developed in Section two, which leads to the following conditions:

$$
\begin{aligned}
&n_\pi = 6\\
&n_\varphi = 3n - 6\\
&{}_\pi\mathbf{W} \text{ is a } 6 \times 6 \text{ real matrix}\\
&\text{rank}({}_\pi\mathbf{W}) = 6
\end{aligned}
$$

When dealing with a set of nonredundant manipulators, the state of a cooperating system (for a given configuration mode) is entirely characterized by the object configuration ($\mathbf{X}^\circ$ and ${}^\circ\mathbf{R}_b$) and by its internal load ($\boldsymbol{\eta}^\circ$). Since the manipulated object has 6 d.o.f. in the 3D space and $\text{rank}({}_\pi\mathbf{W}) = 6$, its configuration is entirely determined by the $n_\pi = 6$ local coordinates corresponding to the purely impedance controlled components. On the other hand, assuming that the system tends toward its desired configuration, the object internal load error also tends to zero as soon as the $n - 6$ force controlled interaction components tend to their desired values. That is only true when ${}_\pi\mathbf{W}$ has no null space and thus position control actions cannot produce any internal force.

To conclude, system stability is ensured as soon as

$$
{}_\pi\mathbf{X} \to {}_\pi\tilde{\mathbf{X}} \quad \text{and} \quad \varphi\mathbf{F} \to \varphi\tilde{\mathbf{F}} \tag{15}
$$

for any initial actual values of $\mathbf{X}^\circ$, ${}^\circ\mathbf{R}_b$, and $\boldsymbol{\eta}^\circ$.

In this section, we establish conditions to satisfy Eq. (15), proceeding in three steps:

1. We define a potential energy function for the system, and show that the configuration ${}_\pi\mathbf{X} = {}_\pi\tilde{\mathbf{X}}$ corresponds to an absolute minimum of this function.

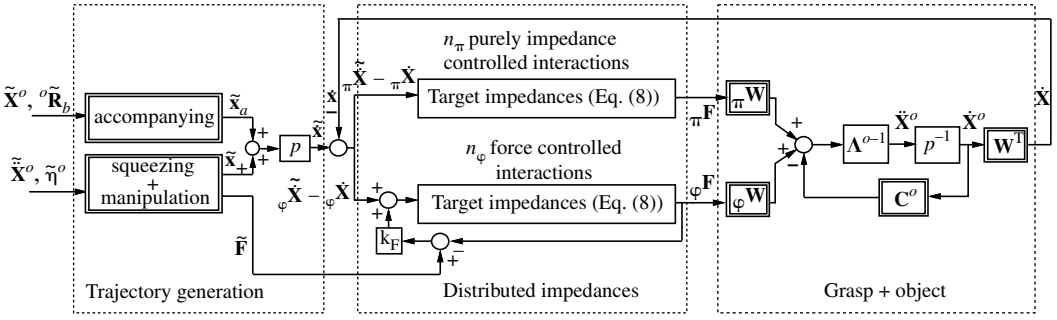

Figure 8. Distributed impedance scheme, including active local force control.

2. Using the hyperstability principle, we demonstrate that ${}_{\varphi}\mathbf{F} \rightarrow {}_{\varphi}\tilde{\mathbf{F}}$, assuming that the different target impedance parameters have been properly chosen.
3. Using results of steps 1 and 2, we show that the desired system configuration is a stable equilibrium point, that is, ${}_{\pi}\mathbf{X} \rightarrow {}_{\pi}\tilde{\mathbf{X}}$.

3.1. System Potential Energy

We define Q as the system potential energy with respect to

- the n_{π} position control actions (programmed stiffness ${}_{\pi}\mathbf{K}$),
- the feedforward applied forces $\tilde{\mathbf{N}}\tilde{\boldsymbol{\eta}}^{\circ}$ and $\tilde{\mathbf{W}}^{\sharp}\tilde{\mathbf{C}}^{\circ}$ (for internal load production and auxiliary effects compensation, respectively), and
- the gravity forces.

So,

$$Q \stackrel{\text{def}}{=} \frac{1}{2}{}_{\pi}\Delta\mathbf{X}^{\mathrm{T}}{}_{\pi}\mathbf{K}\,{}_{\pi}\Delta\mathbf{X} - \Delta\mathbf{X}^{\mathrm{T}}(\tilde{\mathbf{N}}\tilde{\boldsymbol{\eta}} + \tilde{\mathbf{W}}^{\sharp}\tilde{\mathbf{C}}^{\circ}) - m^{\circ}\,\Delta\mathbf{X}^{G\,\mathrm{T}}\,g \tag{16}$$

where $-{}_{\pi}\Delta\mathbf{X} \stackrel{\text{def}}{=} ({}_{\pi}\mathbf{X} - {}_{\pi}\tilde{\mathbf{X}})$, $-\Delta\mathbf{X} \stackrel{\text{def}}{=} (\mathbf{X} - \tilde{\mathbf{X}})$, $-\Delta\mathbf{X}^{G} \stackrel{\text{def}}{=} (\mathbf{X}^{G} - \tilde{\mathbf{X}}^{G})$, and $\mathbf{X}^{G} = \mathbf{X}^{\circ} + \mathbf{G}^{\circ}\mathbf{O}^{\circ}$.

The derivation of Eq. (16) with respect to the system configuration (see Appendix 1) gives

$$\frac{dQ}{d_{\pi}\mathbf{X}^{\mathrm{T}}} = {}_{\pi}\mathbf{K}\,{}_{\pi}\Delta\mathbf{X} - {}_{\pi}\mathbf{W}^{-1}\mathbf{W}\,\tilde{\mathbf{N}}\tilde{\boldsymbol{\eta}} - {}_{\pi}\mathbf{W}^{-1}(\mathbf{W}\,\tilde{\mathbf{W}}^{\sharp} - \mathbf{I\!I}_{6})\,\tilde{\mathbf{C}}^{\circ} \tag{17}$$

Moreover, by the definition of $\tilde{\mathbf{N}}$ and $\tilde{\mathbf{W}}^{\sharp}$, we have

$$\tilde{\mathbf{W}}\,\tilde{\mathbf{N}} = \mathbf{0}_{6\times 3n-6} \quad \text{and} \quad \tilde{\mathbf{W}}\,\tilde{\mathbf{W}}^{\sharp} = \mathbf{I\!I}_{6} \tag{18}$$

Thus, the desired system configuration ${}_{\pi}\Delta\mathbf{X} = 0$ (i.e., $\mathbf{X}^{\circ} = \tilde{\mathbf{X}}^{\circ}$, ${}_{\pi}\mathbf{X} = {}_{\pi}\tilde{\mathbf{X}}$, and $\mathbf{W} = \tilde{\mathbf{W}}$) always verifies that

$$\frac{dQ}{d\,{}_{\pi}\mathbf{X}^{\mathrm{T}}} = 0 \tag{19}$$

When calculating the derivative of Eq. (17) with respect to ${}_{\pi}\mathbf{X}^{\mathrm{T}}$ again, we get

$$\frac{d^{2}Q}{d_{\pi}\mathbf{X}^{\mathrm{T}2}} = {}_{\pi}K - \frac{d({}_{\pi}\mathbf{W}^{-1}\,\mathbf{W})}{d\,{}_{\pi}\mathbf{X}^{\mathrm{T}}}(\tilde{\mathbf{N}}\,\tilde{\boldsymbol{\eta}} + \tilde{\mathbf{W}}^{\sharp}\,\tilde{\mathbf{C}}^{\circ}) + \frac{d\,({}_{\pi}\mathbf{W}^{-1})}{d\,{}_{\pi}\mathbf{X}^{\mathrm{T}}}\,\tilde{\mathbf{C}}^{\circ} \tag{20}$$

Considering the form of matrix $\mathbf{W}$ in Eq. (4), it is obvious that the entries of ${}_{\pi}\mathbf{W}^{-1}$, $\mathbf{W}$, $\tilde{\mathbf{N}}$, and their derivatives with respect to ${}_{\pi}\mathbf{X}$ are bounded. Thus, we can always find a matrix ${}_{\pi}\mathbf{K}^{*}$ such that

$${}_{\pi}\mathbf{K} > {}_{\pi}\mathbf{K}^{*} \Rightarrow \frac{d^{2}Q}{d_{\pi}\mathbf{X}^{\mathrm{T}2}} > 0 \tag{21}$$

This result combined with Eq. (19) indicates that the stiffness matrix ${}_{\pi}\mathbf{K}$ can always be such that the origin $\mathbf{X}^{\circ} = \tilde{\mathbf{X}}^{\circ}$ corresponds to an absolute minimum of the potential energy Q. Moreover, Q is null for $\mathbf{X}^{\circ} = \tilde{\mathbf{X}}^{\circ}$ (Eq. (17)) and positive for any other configuration of the system (Eqs. (19) and (21)).

3.2. Internal Load Stability

Consider now the system shown in Figure 9. It is strictly equivalent to the system in Figure 8, with $\tilde{\mathbf{X}}^{\circ}$ and $\tilde{\boldsymbol{\eta}}^{\circ}$ now considered as constant inputs. Notice that the linearity of relations (13) and (14) allows us to represent the gravity and Coriolis compensation $\tilde{\mathbf{C}}^{\circ}$ and the internal load offset $\tilde{\boldsymbol{\eta}}^{\circ}$ as independent inputs to the system.

The system in Figure 9 is composed of a nonlinear feedback loop enclosing a linear forward block. They are linked through the quantities ${}_{\varphi}\dot{\mathbf{X}}$ and $\Delta_{\varphi}\mathbf{F}$. Here, $\Delta_{\varphi}\mathbf{F} = {}_{\varphi}\mathbf{F} - {}_{\varphi}\tilde{\mathbf{F}}$ is the deviation in applied forces along the force controlled interaction components.

Hyperstability of such a closed loop system is ensured by the strict real positiveness of its forward block and by the passivity of its feedback block.[31]

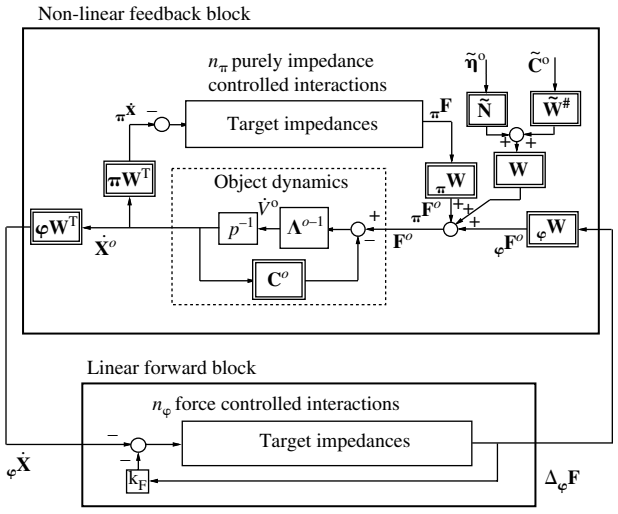

Figure 9. Equivalent closed-loop scheme.

3.2.1. Strict Real Positiveness of the Forward Block

The transfer function associated with the linear forward block is of the form

$$\mathbf{H}(p) = \mathrm{diag}(h^v(p)) \tag{22}$$

$$h^v(p) = \frac{m^v\, p^2 + b^v\, p + k^v}{\left(b^v\, k_F^v + 1\right) p + k^v\, k_F^v} \qquad v = 1, \ldots, n_\varphi \tag{23}$$

where, m^v, b^v, k^v, and k_F^v are parameters of the vth force controlled target impedance.

Thus, strict real positiveness of the forward block is verified as soon as each of the n_φ force controlled object/end-effector interaction components verify that

$$k_F^v > 0, \quad k^v > 0, \quad b^v > 0, \quad m^v > 0 \tag{24}$$

and

$$b^v \left(b^v + \frac{1}{k_F^v} \right) > m^v\, k^v \tag{25}$$

3.2.2. Passivity of the Feedback Block

A sufficient condition for the feedback block to be passive is given by the Popov criterion:[32]

$$\begin{aligned} &\int_0^{\mathrm{T}} ({}_\varphi\dot{\mathbf{X}}^{\mathrm{T}} \Delta_\varphi \mathbf{F})\, dt > -\infty \\ &\quad \Leftrightarrow \int_0^{\mathrm{T}} (\mathbf{V}^{\circ\mathrm{T}}\, {}_\varphi\mathbf{W} \Delta_\varphi \mathbf{F})\, dt > -\infty \\ &\quad \Leftrightarrow \int_0^{\mathrm{T}} (\mathbf{V}^{\circ\mathrm{T}}\, {}_\varphi\mathbf{F}^\circ)\, dt > -\infty \end{aligned} \tag{26}$$

where, ${}_\varphi\mathbf{F}^\circ$ represents the resulting wrench at point $\mathbf{O}^\circ$ exerted by the set of interaction components with force feedback. We show in Appendix 2 that condition (26) is equivalent to

$$\begin{aligned} &\frac{1}{2}\, \mathbf{V}^{\circ\mathrm{T}} \boldsymbol{\Lambda}^\circ \mathbf{V}^\circ + \frac{1}{2} {}_\pi\dot{\mathbf{X}}^{\mathrm{T}}\, {}_\pi\mathbf{M}\, {}_\pi\dot{\mathbf{X}} \\ &+ \int_0^{\mathrm{T}} ({}_\pi\dot{\mathbf{X}}^{\mathrm{T}}\, {}_\pi\mathbf{B}_\pi \dot{\mathbf{X}})\, dt + Q > -\infty \end{aligned} \tag{27}$$

The first term in Eq. (27) is positive because the matrix $\boldsymbol{\Lambda}^\circ$ is positive. The second and third terms are also positive when

$$m^u > 0, \quad b^u > 0 \tag{28}$$

$$u = 1, \ldots, n_\pi \tag{29}$$

for each of the n_π purely impedance controlled components. The fourth term is the system potential energy Q, which is always positive provided that ${}_\pi\mathbf{K}$ has been chosen large enough to verify Eq. (21). Thus, the nonlinear feedback block of the system represented in Figure 9 is passive as soon as conditions (21) and (29) are verified.

These conditions combined with conditions (24) and (25) ensure that the system represented in Figure 9 is passive. Consequently, we have $\Delta_\varphi \mathbf{F} \to 0$, and then

$${}_\varphi\mathbf{F} \to {}_\varphi\tilde{\mathbf{F}} \tag{30}$$

3.3. Stability of the Desired Configuration

Consider now the Lyapunov candidate function

$$G = E_o + E_\pi + Q \tag{31}$$

with

$$E_o = \frac{1}{2} \dot{\mathbf{X}}^{\circ\mathrm{T}} \boldsymbol{\Lambda}^\circ \dot{\mathbf{X}}^\circ \quad \text{and} \quad E_\pi = \frac{1}{2} {}_\pi\dot{\mathbf{X}}_\pi^{\mathrm{T}}\, {}_\pi\mathbf{M}_\pi\, {}_\pi\dot{\mathbf{X}} \tag{32}$$

G is obviously positive for any configuration of the system, and radially unbounded. Moreover, according to Eqs. (8) and (16) and to the results (30), we have

$$\begin{aligned} \frac{d}{dt} E_o &= \dot{\mathbf{X}}^{\circ\mathrm{T}} \boldsymbol{\Lambda}^\circ \ddot{\mathbf{X}}^\circ \\ \frac{d}{dt} E_\pi &= -{}_\pi\dot{\mathbf{X}}_\pi^{\mathrm{T}}\, {}_\pi\mathbf{B}_\pi\, {}_\pi\dot{\mathbf{X}} - {}_\pi\dot{\mathbf{X}}_\pi^{\mathrm{T}}\, {}_\pi\mathbf{K}_\pi\, {}_\pi\mathbf{X} - \dot{\mathbf{X}}^{\circ\mathrm{T}} \boldsymbol{\Lambda}^\circ \ddot{\mathbf{X}}^\circ - \dot{\mathbf{X}}^{\circ\mathrm{T}} \mathbf{A}({}_\pi\mathbf{X}) \\ \frac{d}{dt} Q &= {}_\pi\dot{\mathbf{X}}_\pi^{\mathrm{T}}\, {}_\pi\mathbf{K}_\pi\, {}_\pi\mathbf{X} - \Delta\dot{\mathbf{X}}^{\circ\mathbf{T}} \mathbf{W}(\tilde{\mathbf{N}}\tilde{\boldsymbol{\eta}}_0 + \tilde{\mathbf{W}}^\sharp \tilde{\mathbf{C}}^\circ) - m^\circ\, \dot{\mathbf{X}}^{G\mathrm{T}}\, \boldsymbol{g} \\ &= {}_\pi\dot{\mathbf{X}}_\pi^{\mathrm{T}}\, {}_\pi\mathbf{K}_\pi\, {}_\pi\mathbf{X} + \dot{\mathbf{X}}^{\circ\mathrm{T}} \mathbf{A}({}_\pi\mathbf{X}) \end{aligned}$$

with

$$\mathbf{A}({}_\pi\mathbf{X}) \stackrel{\mathrm{def}}{=} \mathbf{C}^\circ - \mathbf{W}(\tilde{\mathbf{N}}\tilde{\boldsymbol{\eta}}_0 + \tilde{\mathbf{W}}^\sharp \tilde{\mathbf{C}}^\circ) \tag{33}$$

Summing the time derivatives above, we find that

$$\dot{G} = -\, {}_\pi\dot{\mathbf{X}}^{\mathrm{T}}\, {}_\pi\mathbf{B}_\pi\, {}_\pi\dot{\mathbf{X}} \tag{34}$$

which is always negative or null.

According to Lassale's theorem, the system converges and remains in the largest subset of ${}_\pi\mathbf{X}$, such that

$$\dot{G} = 0 \tag{35}$$

We now shall prove that the system is globally asymptotically stable; that is, the subset defined by (35) is reduced to the desired state ${}_{\pi}\tilde{\mathbf{X}}$.

First, since ${}_{\pi}\mathbf{B}$ is nonsingular, (35) is equivalent to ${}_{\pi}\dot{\mathbf{X}} = 0$, which in turn is equivalent to $\mathbf{V}^{\circ} = 0$ as $\mathbf{V}^{\circ} = {}_{\pi}\mathbf{W}^{-\mathrm{T}}\,{}_{\pi}\dot{\mathbf{X}}$. In Appendix 3, we show that $\mathbf{V}^{\circ} = 0$ implies

$$-{}_{\pi}\mathbf{W}_{\pi}\mathbf{K}_{\pi}\,\Delta\mathbf{X} + \mathbf{W}(\tilde{\mathbf{N}}\tilde{\boldsymbol{\eta}} + \tilde{\mathbf{W}}^{\sharp}\tilde{\mathbf{C}}^{\circ}) - \tilde{\mathbf{C}}^{\circ} = \mathbf{0}_{6\times 1} \quad (36)$$

Multiplying each side of (36) by ${}_{\pi}\mathbf{W}^{-1}$, we get

$${}_{\pi}\mathbf{K}_{\pi}\Delta\mathbf{X} - {}_{\pi}\mathbf{W}^{-1}\mathbf{W}\tilde{\mathbf{N}}\tilde{\boldsymbol{\eta}}_{-{}_{\pi}}\mathbf{W}^{-1}(\mathbf{W}\tilde{\mathbf{W}}\mathbf{W}^{\sharp} - \mathbb{I})\tilde{\mathbf{C}}^{\circ} = \mathbf{0}_{6\times 1} \quad (37)$$

This last result, introduced into (17), gives

$$\frac{dQ}{d\,{}_{\pi}\mathbf{X}} = 0$$

which has been proven in Section 3.1 to be equivalent to

$${}_{\pi}\mathbf{X} = {}_{\pi}\tilde{\mathbf{X}} \quad \text{or} \quad \mathbf{X}^{\circ} = \tilde{\mathbf{X}}^{\circ}$$

3.4. Conclusion

In this section, we have determined sufficient conditions for the distributed impedance controller of Figure 8 to be stable. Practically, object configuration and internal load will tend toward their desired values with no steady-state error as soon as

- we ensure the real positiveness of the force control through conditions (24) and (25), and
- we choose stiffness parameters of position controlled interactions sufficiently high, such that ${}_{\pi}\mathbf{K} > {}_{\pi}\mathbf{K}^{*}$ (condition (21)).

4. EXPERIMENTAL SETUP

Distributed impedance control has been applied to an experimental dual arm cell, involving an IBM 7576 Scara and a Puma 560 manipulator (Figure 10(a)). Each manipulator is featured with a six-axis force/torque sensor, and fingers with sharp extremities that establish frictional and almost punctual contacts with the manipulated object.

Each manipulator uses a VME bus–based independent controller. Real-time control of motions and applied forces is implemented at a 5 ms sampling rate on two Motorola 68020 CPUs. Software development was achieved using C language programs on a standard personal computer. Only the reference trajectory computation is common to the two subsystems.

5. DYNAMIC TRANSPORTATION TASK

The first experiment consists in transporting an object (15 cm × 5 cm × 3 cm, 0.5 kg) in a horizontal plane (Figure 10(b)). In such a planar case, we have shown (Section 2) that four object/manipulator interaction components must be controlled (Figure 7(a)). Three components of at least $n_{\pi} \geq 3$ must be purely impedance controlled, while the remaining component is featured with a force control loop. Thus, the repartition shown in Figure 7(c) is applied here. The y- component of the interaction with the SCARA is selected to be force controlled.

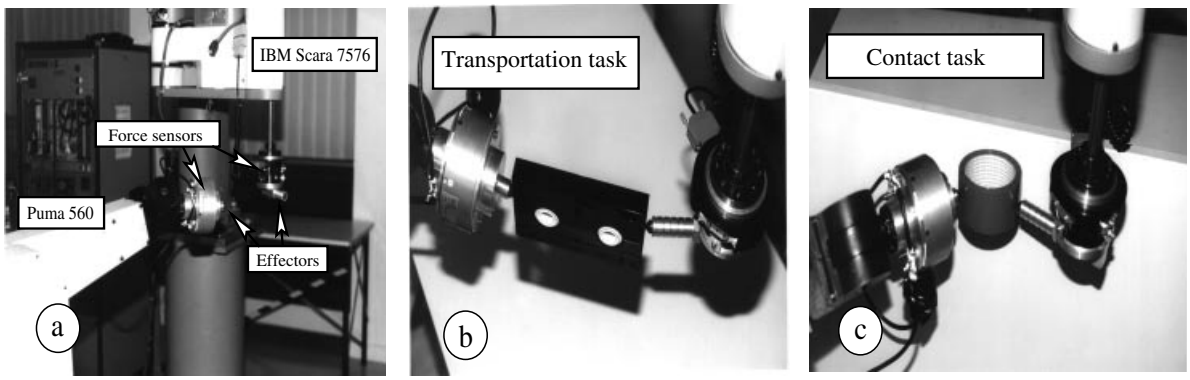

Figure 10. Experimental setup and task realizations.

5.1. Stability considerations

In case of the grasp of Figure 7(a), and when contact frames are correctly oriented with respect to the object (Figure 11(a)), the grasp matrix $\mathbf{W}$ has the ideal form

$$\mathbf{W} = \tilde{\mathbf{W}} = \begin{pmatrix} \cos(\theta) & -\sin(\theta) & -\cos(\theta) & \sin(\theta) \\ \sin(\theta) & \cos(\theta) & -\sin(\theta) & -\cos(\theta) \\ r & 0 & r & 0 \end{pmatrix} \tag{38}$$

where r is the object half-length and θ the object orientation in the plane. In this case, a base for the null space of $\mathbf{W}$ is given by the vector $\mathbf{N} = \tilde{\mathbf{N}} = (0\ 1\ 0\ 1)^{\mathrm{T}}$.

When the object deviates from its desired orientation ($\delta\theta = \tilde{\theta} - \theta \neq 0$), contact frames are no longer correctly oriented with respect to the object (Figure 11(b)) and the grasp matrix $\mathbf{W}$ becomes

$$\mathbf{W} = \begin{pmatrix} \cos(\theta) & -\sin(\theta) & -\cos(\theta) & \sin(\theta) \\ \sin(\theta) & \cos(\theta) & -\sin(\theta) & -\cos(\theta) \\ r\cos(\delta\theta) & r\sin(\delta\theta) & r\cos(\delta\theta) & r\sin(\delta\theta) \end{pmatrix} \tag{39}$$

As we can see, the resulting applied moment, which depends on the last row of $\mathbf{W}$, is affected. Moreover, within the context of a decentralized control scheme, the actual object orientation error $\delta\theta$ can not be evaluated in-line. Indeed, from the single manipulator point of view, the only available piece of information concerning the object configuration is the location of the corresponding contact point on the object surface. Thus, in-line compensation of the aforementioned grasp matrix discrepancy (through, for example, a suitable in-line adaptation of the commanded efforts $\tilde{\mathbf{F}}^i$) is not possible. This makes the system very sensitive to object angular deviations.

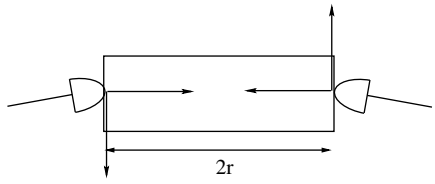

(a) Zero angular deviation ($\boldsymbol{\delta\theta} = 0$)

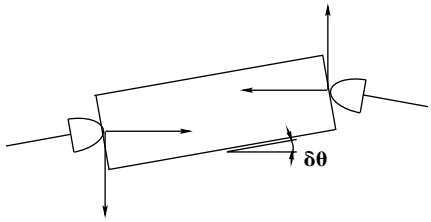

(b) Nonzero angular deviation ($\boldsymbol{\delta\theta} \neq 0$)

Figure 11. Influence of object angular positioning.

However, according to the proposed grasp repartition, the submatrices ${}_{\pi}\mathbf{W}$ and ${}_{\varphi}\mathbf{W}$ extracted from $\mathbf{W}$ are

$${}_{\pi}\mathbf{W} = \begin{pmatrix} \cos(\theta) & -\cos(\theta) & \sin(\theta) \\ \sin(\theta) & -\sin(\theta) & -\cos(\theta) \\ r\cos(\delta\theta) & r\cos(\delta\theta) & r\sin(\delta\theta) \end{pmatrix} \tag{40}$$

$${}_{\varphi}\mathbf{W} = \begin{pmatrix} -\sin(\theta) \\ \cos(\theta) \\ r\sin(\delta\theta) \end{pmatrix} \tag{41}$$

Note that ${}_{\pi}\mathbf{W}$ remains nonsingular as long as $\delta\theta < 90^{\circ}$, which is always true in practice.

Moreover, since for this planar horizontal case gravity is not involved, condition (21) relative to the system stability yields

$$\begin{pmatrix} k_x^1 & 0 & 0 \\ 0 & k_x^2 & 0 \\ 0 & 0 & k_y^2 \end{pmatrix} - \frac{d\,({}_{\pi}\mathbf{W}^{-1}\mathbf{W})}{d\theta}\,\frac{d\theta}{d\,{}_{\pi}\mathbf{X}}\bigg|_{\substack{\mathbf{X}^{\circ} = \tilde{\mathbf{X}}^{\circ} \\ \theta = \tilde{\theta}}} \tilde{\mathbf{N}}\,\tilde{\boldsymbol{\eta}}^{\circ} > 0 \tag{42}$$

According to (41), this inequality can be reduced to

$${}_{\pi}\mathbf{K} = \begin{pmatrix} k_x^1 & 0 & 0 \\ 0 & k_x^2 & 0 \\ 0 & 0 & k_y^2 \end{pmatrix} > \begin{pmatrix} k_x^1 - \frac{\tilde{\eta}^{\circ}}{2r} & -\frac{\tilde{\eta}^{\circ}}{2r} & 0 \\ -\frac{\tilde{\eta}^{\circ}}{2r} & k_x^2 - \frac{\tilde{\eta}^{\circ}}{2r} & 0 \\ 0 & 0 & k_y^2 \end{pmatrix} = {}_{\pi}\mathbf{K}^{*} \tag{43}$$

which is verified when

$$\frac{k_x^1 k_x^2}{k_x^1 + k_x^2} > \frac{\tilde{\eta}^{\circ}}{2r} \quad \text{and} \quad k_y^2 > 0 \tag{44}$$

From a physical point of view, the first inequality in (44) can be interpreted as a condition on the serial combination of the two tangential stiffnesses k_x^1 and k_x^2. Equation (44) also implies that $k_x^1 + k_x^2 > 2\,\eta^{\circ}/r$, which is, in turn, a condition on the parallel combination of k_x^1 and k_x^2. Practically, this combination must overcome the angular destabilizing effect of the object internal loading η°. As we can see, increasing the object width $2r$ increases stability boundaries.

Table I. Parameter Tuning for Transportation Task.

	m^i_β (Ns^2/m)	k^i_β (N/m)	b^i_β (Ns/m)	$k^i_{F_\beta}$ (m/sN)
F^1_x	30–60	18900	1260	0
F^1_y	30–60	6200	1930	$7 \cdot 10^{-3}$
F^2_x	40–60	5400	85	0
F^2_y	40–60	6100	170	0

5.2. Tuning of the Controllers

The controller parameters are fixed according to the following four-steps reasoning.

1. Individual target impedances are initialized at values that consider manipulators performing independent tasks.
2. These values are then adjusted according to the type of closed kinematic chain constituted. Particular attention must be paid to the apparent impedance reflected at each contact point.
3. Preliminary tests have been achieved along elementary trajectories leading to an empirical final adjustment of impedance parameters and force feedback gains.
4. We then check that stability requirements (25) and (21) are met.

Applying this reasoning to the transportation task of Figure (10(b)), we obtain the set of parameters given in Table I.

5.3. Results

Here, the object trajectory involves both linear and angular object motions within a wide range of velocities and accelerations (the dotted lines in Figure 12(b–d)). The path of the object center of mass is a horizontal square interpolated using a fifth-order polynomial profile. Its orientation has a 20-degree alternative motion. The desired internal force is set to 12 N. Individual reference trajectories are computed according to task specification and Eqs. (11–14), and the kinematic redundancy of the system is solved by choosing a constant orientation of the two end-effectors while the task is performed.

Figure 12 shows results in trajectory tracking and internal force regulation. With linear and angular errors less than 1 mm and 0.03 radian, respectively, the trajectory is accurately followed. Internal load (Figure 12(a)) has been filtered for noise measurement attenuation using a low-pass filter with 30 Hz

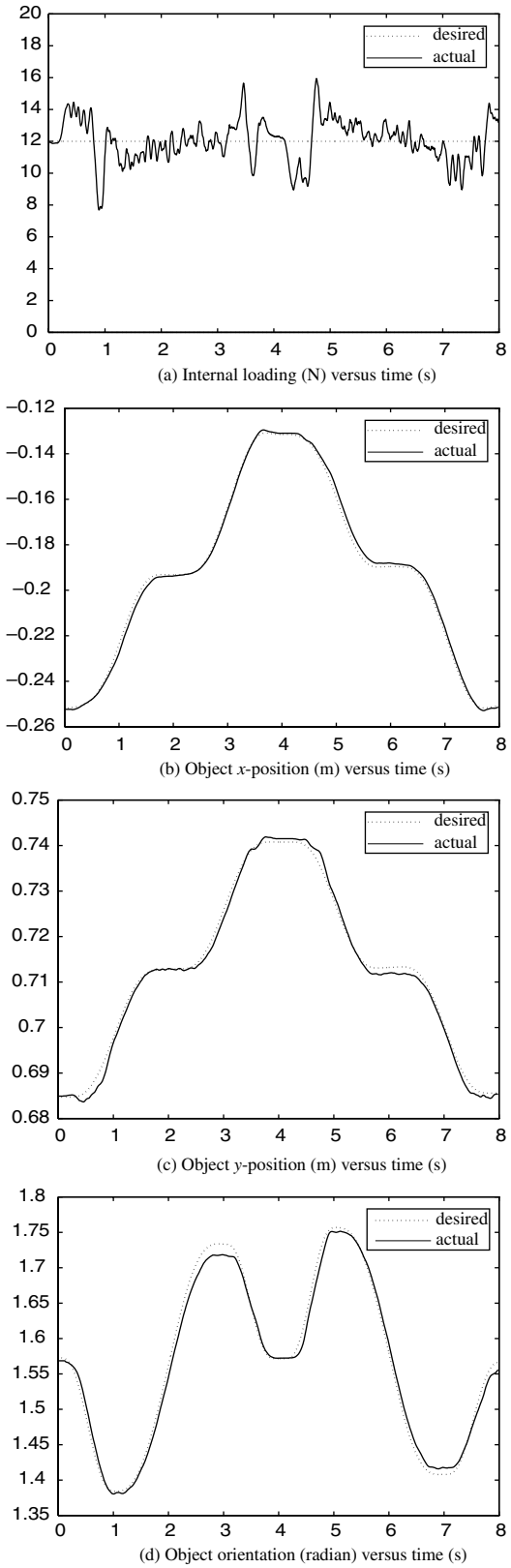

Figure 12. Results of the transportation task.

bandwidth. The largest errors occur when the system starts or completely stops (i.e., beginning, middle, and end of the trajectory). This is mainly due to important joint stiction effects. Anywhere else (and particularly for phases at maximal velocity), internal load is correctly regulated.

6. CONTACT TASK

To illustrate the generality and flexibility of the distributed impedance approach, we also performed a contact task using the same dual-arm cooperative cell, without any modification in the controller structure. This task is illustrated in Figure 10(c). The manipulated object is a rigid cylinder with radius 0.05 m. It comes into contact with a planar, vertical, rigid surface. Since there is no friction between the object and the environment, the applied external force $\mathbf{F}_{\text{ext}}$ is normal to the contact surface (Figure 7(b)).

As depicted in Figure 7(d), two active force-control loops can be implemented here. They are applied along the two y-directions of the two contact frames. They match the directions of contact forces needed for producing both the object internal force (12 N) and the desired contact force $\mathbf{F}_{\text{ext}}$ (between 0.5 N and 7.5 N). Because $\mathbf{F}_{\text{ext}}$ changes during the task, contact-frame orientations also change.

6.1. Tuning of the Controllers

Controller parameters are tuned based on the same reasoning used for the transportation task. Here, we just consider the contact between the object and the environment as an additional object-effector interaction involving an infinite target impedance in the direction normal to the contact and a null impedance in its tangential direction.

We obtain the parameters given in Table II.

6.1.1. Results

The object internal and contact forces that we obtain are represented in Figure 13. As we can see, both forces

Table II. Parameter Tuning for Contact Task.

	m^i_β (Nm/s^2)	k^i_β (N/m)	b^i_β (Ns/m)	$k^i_{F_\beta}$ (m/sN)
f^1_x	30–60	5800	630	0
f^1_y	30–60	5800	630	$7 \cdot 10^{-3}$
f^2_x	40–60	5400	85	0
f^2_y	40–60	5400	85	$6 \cdot 10^{-3}$

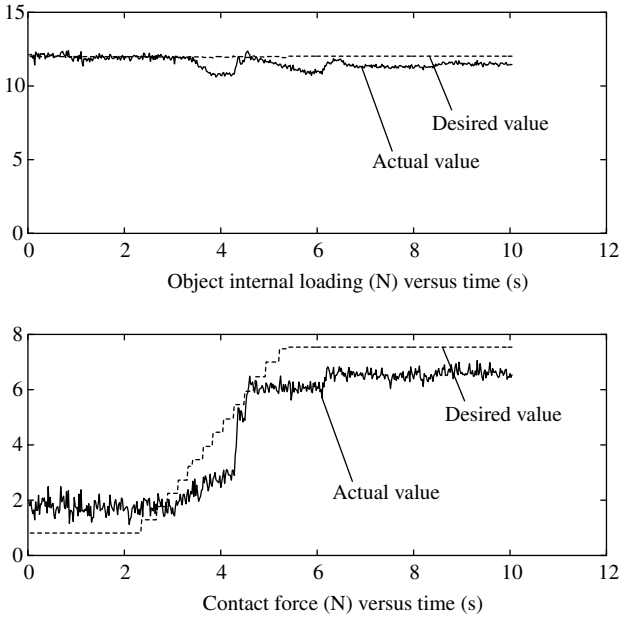

Figure 13. Results for the contact task.

are correctly regulated around their desired values, with final deviation less than 1 N in both cases.

7. CONCLUSION

In this article, a distributed impedance approach is proposed to solve the problem of controlling cooperative systems (such as multiarm systems or articulated hands.)

Details of the implementation are discussed, considering the example of an object being grasped through a set of punctual frictional contacts. An extended stability analysis is performed based on the hyperstability principle. Finally, experimental results are presented for different kinds of manipulation tasks performed with a Scara-Puma dual-arm system.

Distributed impedance is basically a decentralized control approach. Thus, it provides simplicity and modularity in hardware development and task planning over centralized solutions. In this article, for example, the same controller is used to achieve a dynamic free transporation task and a static task where the object comes into contact with a rigid environment.

Moreover, impedance control is implemented at the end-effector level. Thus, it also provides an efficient regulation of object-effector interactions. Particularly, it allows the introduction of a local, active force control at the object-effector interface. This brings robustness in object internal force control while the object position is still controlled in a closed loop.

APPENDIX 1

Deriving Eq. (16) with respect to ${}_{\pi}\mathbf{X}$, we find

$$\frac{dQ}{d_{\pi}\mathbf{X}^{\mathrm{T}}} = {}_{\pi}\mathbf{K}\,{}_{\pi}\Delta\mathbf{X} - \frac{d\mathbf{X}^{\mathrm{T}}}{d_{\pi}\mathbf{X}^{\mathrm{T}}}(\tilde{\mathbf{N}}\tilde{\boldsymbol{\eta}} + \tilde{\mathbf{W}}^{\sharp}\,\tilde{\mathbf{C}}^{\circ}) - m^{\circ}\frac{d\mathbf{X}^{\mathrm{GT}}}{d_{\pi}\mathbf{X}^{\mathrm{T}}}g$$

Regarding (5), and the fact that ${}_{\pi}\mathbf{W}$ (which is extracted from $\mathbf{W}$) is a 6×6 full rank matrix, yields

$$\dot{\mathbf{X}} = \mathbf{W}^{\mathrm{T}}\,{}_{\pi}\mathbf{W}^{-\mathrm{T}}\,{}_{\pi}\dot{\mathbf{X}} \tag{45}$$

Moreover, because the components of ${}_{\pi}\mathbf{X}$ constitute a set of generalized coordinates for the system, we have

$$\dot{\mathbf{X}} = \frac{d\mathbf{X}}{d_{\pi}\mathbf{X}}\,{}_{\pi}\dot{\mathbf{X}} \tag{46}$$

Comparing (45) and (46) gives

$$\left(\frac{d\mathbf{X}^{\mathrm{T}}}{d_{\pi}\mathbf{X}^{\mathrm{T}}}\right)^{\mathrm{T}} = \frac{d\mathbf{X}}{d_{\pi}\mathbf{X}} = \mathbf{W}^{\mathrm{T}}\,{}_{\pi}\mathbf{W}^{-\mathrm{T}} \tag{47}$$

Similarly to (46), we can write

$$\dot{\mathbf{X}}^{G} = \frac{d\mathbf{X}^{G}}{d_{\pi}\mathbf{X}}\,{}_{\pi}\dot{\mathbf{X}} \tag{48}$$

On the other hand, we have

$$\dot{\mathbf{X}}^{G} = \frac{d}{dt}(\mathbf{X}^{\circ} + \mathbf{O}^{\circ}\mathbf{G}^{\circ}) = \dot{\mathbf{X}}^{\circ} + (\dot{\mathbf{O}^{\circ}\mathbf{G}^{\circ}}) \tag{49}$$

and

$$(\dot{\mathbf{O}^{\circ}\mathbf{G}^{\circ}}) = \boldsymbol{\Omega}^{\circ} \times \mathbf{O}^{\circ}\mathbf{G}^{\circ} = \mathbf{S}(\mathbf{O}^{\circ}\mathbf{G}^{\circ})\boldsymbol{\Omega}^{\circ} \tag{50}$$

Thus,

$$\dot{\mathbf{X}}^{G} = (\mathbb{I}_3,\, \mathbf{S}(\mathbf{O}^{\circ}\mathbf{G}^{\circ}))\,\mathbf{V}^{\circ} = (\mathbb{I}_3,\, \mathbf{S}(\mathbf{O}^{\circ}\mathbf{G}^{\circ}))_{\pi}\mathbf{W}^{-\mathrm{T}}\,{}_{\pi}\dot{\mathbf{X}} \tag{51}$$

Comparing (48) with (51) leads to

$$\left(\frac{d\mathbf{X}^{\mathrm{GT}}}{d_{\pi}\mathbf{X}^{\mathrm{T}}}\right)^{\mathrm{T}} = \frac{d\,\mathbf{X}^{G}}{d\,{}_{\pi}\mathbf{X}} = (\mathbb{I}_3,\, \mathbf{S}(\mathbf{O}^{\circ}\mathbf{G}^{\circ}))_{\pi}\mathbf{W}^{-\mathrm{T}} \tag{52}$$

and then, according to (3),

$$\begin{aligned} m^{\circ}\frac{d\,\mathbf{X}^{\mathrm{GT}}}{d\,{}_{\pi}\mathbf{X}^{\mathrm{T}}}\,g &= {}_{\pi}\mathbf{W}^{-1}(\mathbb{I}_3,\, \mathbf{S}(\mathbf{O}^{\circ}\mathbf{G}^{\circ}))^{\mathrm{T}} m^{\circ} g \\ &= {}_{\pi}\mathbf{W}^{-1}\begin{pmatrix} m^{\circ} g \\ \mathbf{S}(\mathbf{O}^{\circ}\mathbf{G}^{\circ}) m^{\circ} g \end{pmatrix} = -{}_{\pi}\mathbf{W}^{-1}\tilde{\mathbf{C}}^{\circ} \end{aligned} \tag{53}$$

Introducing (53) and (47) into (45) gives (17).

APPENDIX 2

Summation at the entrance of the nonlinear block of Figure 9 yields

$$\mathbf{W}\,(\tilde{\mathbf{N}}\tilde{\boldsymbol{\eta}}^{\circ} + \tilde{\mathbf{W}}^{\sharp}\,\tilde{\mathbf{C}}^{\circ}) + {}_{\pi}\mathbf{F}^{\circ} + {}_{\varphi}\mathbf{F}^{\circ} = \boldsymbol{\Lambda}^{\circ}\,\dot{\mathbf{V}}^{\circ} + \mathbf{C}^{\circ} \tag{54}$$

which is equivalent to

$${}_{\varphi}\mathbf{F}^{\circ} = -\mathbf{W}(\tilde{\mathbf{N}}\tilde{\boldsymbol{\eta}}^{\circ} + \tilde{\mathbf{W}}^{\sharp}\,\tilde{\mathbf{C}}^{\circ}) - {}_{\pi}\mathbf{F}^{\circ} + \boldsymbol{\Lambda}^{\circ}\,\dot{\mathbf{V}}^{\circ} + \mathbf{C}^{\circ} \tag{55}$$

On the other hand, we have also (eq. 3 and 8).

$$-{}_{\pi}\mathbf{F}^{\circ} = {}_{\pi}\mathbf{W}({}_{\pi}\mathbf{M}_{\pi}\ddot{\mathbf{X}} + {}_{\pi}\mathbf{B}_{\pi}\dot{\mathbf{X}} + {}_{\pi}\mathbf{K}\,{}_{\pi}\Delta\mathbf{X}) \tag{56}$$

Introducing (55), (56), and the relation $\mathbf{V}^{\circ\mathrm{T}} = {}_{\pi}\dot{\mathbf{X}}^{\mathrm{T}}\,{}_{\pi}\mathbf{W}^{-1}$ into (26) gives the condition

$$\begin{aligned} \int_0^t \big[\mathbf{V}^{\circ\mathrm{T}}\boldsymbol{\Lambda}^{\circ}\,\dot{\mathbf{V}}^{\circ} + \mathbf{V}^{\circ\mathrm{T}}\mathbf{C}^{\circ} + {}_{\pi}\dot{\mathbf{X}}^{\mathrm{T}}({}_{\pi}\mathbf{M}_{\pi}\ddot{\mathbf{X}} + {}_{\pi}\mathbf{B}_{\pi}\dot{\mathbf{X}} \\ + {}_{\pi}\mathbf{K}\,{}_{\pi}\Delta\mathbf{X}) - \dot{\mathbf{X}}^{\mathrm{T}}(\tilde{\mathbf{N}}\,\tilde{\boldsymbol{\eta}}^{\circ} + \tilde{\mathbf{W}}^{\sharp}\,\tilde{\mathbf{C}}^{\circ})\big]\,dt > -\infty \end{aligned} \tag{57}$$

Moreover, using the definition of $\tilde{\mathbf{C}}^{\circ}$ in (2), we have

$$\begin{aligned} \int_0^t \mathbf{V}^{\circ\mathrm{T}}\mathbf{C}^{\circ}\,dt &= \int_0^t -m^{\circ}\,\dot{\mathbf{X}}^{\circ\mathrm{T}} g - m^{\circ}\,\mathbf{G}^{\circ}\mathbf{O}^{\circ} \times \boldsymbol{\Omega}^{\circ\mathrm{T}} g\,dt \\ &= \int_0^t -m^{\circ}\,\dot{\mathbf{X}}^{\mathrm{GT}} g\,dt \\ &= -m^{\circ}\,\Delta\mathbf{X}^{\mathrm{GT}} g \end{aligned} \tag{58}$$

and (58) combined with (57) gives (27).

APPENDIX 3

Introducing ${}_{\pi}\dot{\mathbf{X}} = 0$ and ${}_{\pi}\ddot{\mathbf{X}} = 0$ into (56) gives

$$-{}_{\pi}\mathbf{F}^{\circ} = {}_{\pi}\mathbf{W}\,{}_{\pi}\mathbf{K}\,{}_{\pi}\Delta\mathbf{X} \tag{59}$$

Moreover, we have shown that commanded forces ${}_{\varphi}\mathbf{F}$ tend to their desired values, which implies that

$${}_{\varphi}\mathbf{F}^{\circ} = {}_{\varphi}\mathbf{W}\,\Delta_{\varphi}\mathbf{F} = \mathbf{0}_{6\times 1} \tag{60}$$

Introducing (59) and (60) into (54) gives

$$\mathbf{W}(\tilde{\mathbf{N}}\tilde{\boldsymbol{\eta}}^{\circ} + \tilde{\mathbf{W}}^{\sharp}\,\tilde{\mathbf{C}}^{\circ}) - {}_{\pi}\mathbf{W}\,{}_{\pi}\mathbf{K}\,{}_{\pi}\Delta\mathbf{X} = \boldsymbol{\Lambda}^{\circ}\,\dot{\mathbf{V}}^{\circ} + \mathbf{C}^{\circ} \tag{61}$$

Finally, because the object is at rest, we have $\dot{\mathbf{V}}^{\circ} = \mathbf{0}_{6\times 1}$ and $\tilde{\mathbf{C}}^{\circ} = \mathbf{C}^{\circ}$ (see the definition of $\mathbf{C}^{\circ}$ in (2)), and then,

$$-{}_{\pi}\mathbf{W}\,{}_{\pi}\mathbf{K}\,{}_{\pi}\Delta\mathbf{X} + \mathbf{W}(\tilde{\mathbf{N}}\tilde{\boldsymbol{\eta}} + \tilde{\mathbf{W}}^{\sharp}\,\tilde{\mathbf{C}}^{\circ}) - \tilde{\mathbf{C}}^{\circ} = \mathbf{0}_{6\times 1} \quad (62)$$

REFERENCES

1. O. Khatib, Inertial properties in robotic manipulation: An object-level framework, Int J Robot Res 13:(1) (1995), 19–36.
2. S.A. Hayati, Position and force control of coordinated multiple arms, IEEE Trans Aerospace Electronic Syst 24:(5) (1988), 584–590.
3. M. Uchiyama and P. Dauchez, Symmetric kinematic formulation and non-master/slave coordinated control of two-arm robots, Advanced Robotics 7:(4) (1989), 361–383.
4. T. Yoshikawa and X. Zheng, Coordinated dynamic hybrid position/force control for multiple robot manipulators handling one constrained object, Int J Robot Res 12:(3) (1993), 219–230.
5. W.H. Zhu and J. DeSchutter, Experiment with two industrial robot manipulators rigidly holding an egg, Proc IEEE Int Conf on Robotics and Automation, 1998, pp. 1534–1539.
6. Z. Li, P. Hsu, and S. Sastry, On grasping and dynamic coordination of multifingered robot hand, Internal report, Electronics Research Laboratory, University of California, 1987.
7. P. Hsu, Coordinated control of multiple manipulator systems, IEEE Trans Robot Automat 9:(4) (1993), 400–410.
8. S.A. Schneider and R. H. Cannon, Object impedance control for cooperative manipulation: Theory and experimental results, IEEE Trans Robot Automat 8:(3) (1992), 383–394.
9. K. Nagai, S. Iwasa, K. Watanabe, and H. Hanafusa, Cooperative control of dual-arm robots for reasonable motion distribution, Proc IEEE Int Conf on Intelligent Robots and Systems, 1995, pp. 54–61.
10. P. Chiacchio, S. Chiaverini, L. Sciavicco, and B. Siciliano, Dynamic force/motion control of cooperative robot systems, Proc ASME Winter Annual Meeting, 1990, pp. 121–126.
11. F. Caccavale, S. Chiaverini, C. Natale, B. Siciliano, and L. Villani, Geometrically consistent impedance control for dual-robot manipulation, Proc IEEE Int Conf on Robotics and Automation, 2000, pp. 3874–3879.
12. H.R. Choi and W.K.C.Y. Youm, Control of grasp stiffness using a multifingered hand with redundant joint, Robotica 13 (1995), 351–362.
13. S. Arimoto, F. Miyazaki, and S. Kawamura, Cooperative motion control of multiple robot arms or fingers, Proc IEEE Int Conf on Robotics and Automation, 1987, pp. 1407–1412.
14. Y.F. Zheng and J.Y.S. Luh, Joint torques for control of two coordinated moving robots, Proc IEEE Int Conf on Robotics and Automation, 1986, pp. 1375–1380.
15. C.O. Alford and S.M. Belyeu, Coordinated control of two robot arms, Proc IEEE Int Conf on Robotics and Automation, 1984, pp. 468–473.
16. K.I. Kim and Y.F. Zheng, Two strategies of position and force control for two industrial robots handling a single object, Robot Autonomous Syst 5 (1989), 395–403.
17. V. Perdereau and M. Drouin, Hybrid external control for two robot coordinated motion, Robotica 14 (1996), 141–153.
18. S. Chiaverini and L. Sciavicco, The parallel approach to force/position control of robotic manipulators, IEEE Trans Robot Automat 9:(4) (1993), 361–373.
19. H. Kazerooni, K.G. Bouklas, and J.Guo, Theory and experiments on the compliance control of redundant robot manipulators, J Dyn Syst Meas Contr 112 (1990), 653–660.
20. T.A. Lasky and T.C. Hsia, On force-tracking impedance control of robot manipulators, Proc IEEE Int Conf on Robotics and Automation, 1991, pp. 274–280.
21. G. Morel and P. Bidaud, A reactive external force loop approach to control manipulators in the presence of environmental disturbances, Proc IEEE Int Conf on Robotics and Automation, 1996, pp. 1229–1234.
22. R.G. Bonitz and T.C. Hsia, Internal force-based impedance control for cooperating manipulators, IEEE Trans Robot Automat 12:(1) (1996), 78–89.
23. S. Moosavian and E. Papadopoulos, On the control of space free-flyers using multiple impedance control, Proc IEEE Int Conf on Robotics and Automation, 1997, pp. 853–858.
24. K. Kosuge, M. Koga, K. Furuta, and K. Nosaki, Coordinated motion control of robot arm based on virtual internal model, Proc IEEE Int Conf on Robotics and Automation, 1989, pp. 1097–1102.
25. Y. Nakamura, K. Nagai, and T. Yoshikawa, Dynamics and stability in coordination of multiple robotic mechanisms, Int J Robot Res 8:(2) (1989), 44–61.
26. J. Szewczyk and P. Bidaud, A force-closure measure for grasps under distributed impedance control, Proc 12th Symposium on Theory and Practice of Robots and Manipulators, 1998.
27. H. Ishikawa, C. Sawada, K. Kawase, and M. Takata, Stable compliance control and its implementation for a 6 d.o.f. manipulator, Proc IEEE Int Conf on Robotics and Automation, 1989, pp. 98–103.
28. D.A. Lawrence, Impedance control stability properties in common implementations, Proc IEEE Int Conf on Robotics and Automation, 1985, pp. 1185–1189.
29. N. Hogan, Impedance control : An approach to manipulation, J Dyn Syst Meas Contr 107 (1985), 1–24.
30. V. Nguyen, Constructing a stable grasp in three dimensional, Proc IEEE Int Conf on Robotics and Automation, 1987, pp. 234–239.
31. K.S. Narendra and L.S. Valavani, A comparison of Lyapunov and hyperstability approaches to adaptive control of continuous systems, IEEE Trans Automat Contr 25:(2) (1980), 243–247.
32. H.K. Khalil, Nonlinear systems, MacMillan, 1989.